

# We are IntechOpen, the world's leading publisher of Open Access books Built by scientists, for scientists

6,900

Open access books available

186,000

International authors and editors

200M

Downloads

Our authors are among the

154

Countries delivered to

TOP 1%

most cited scientists

12.2%

Contributors from top 500 universities



WEB OF SCIENCE™

Selection of our books indexed in the Book Citation Index  
in Web of Science™ Core Collection (BKCI)

Interested in publishing with us?  
Contact [book.department@intechopen.com](mailto:book.department@intechopen.com)

Numbers displayed above are based on latest data collected.  
For more information visit [www.intechopen.com](http://www.intechopen.com)



---

# Research on Simulation and Casting of Mechanical Parts Made of Wear-and-Tear-Resistant Steels

---

Ioan Ruja, Constantin Marta,  
Doina Frunzăverde and Monica Roșu

Additional information is available at the end of the chapter

<http://dx.doi.org/10.5772/50563>

---

## 1. Introduction

The conversion of hydraulic energy into electrical energy is not polluting, supposes relatively small upkeep expenses, and there are no problems related to fuel; it constitutes thus a long-term solution. Hydroelectric power plants have the lowest exploitation costs and the longest life duration compared to other types of electric power plants. These hydroelectric power plants use several types of turbines, and the Kaplan turbine is the most frequently used. The Kaplan turbine is a hydraulic turbine with axial rotation, with an adjustable-blades rotor, used in small-fall hydroelectric power plants, i.e.  $H= 10 - 50$  metres and  $Q=(700-800) \text{ m}^3/\text{s}$ . At present, the equipment of hydroelectric power plants which meets the above parameter requirements is mainly endowed with Kaplan turbines. The researches of specialists in the construction of these turbines are focused on the turbines' configuration and physical dimensions, on reaching high hydro-energetic parameters, as well as on the increase of these turbines' life duration. The preoccupations of the research team who conducted the present study fall within this context, for the purpose of getting optimum technical results by improving the casting conditions of the main parts in the structure of the Kaplan turbine, more precisely the rotor block and the blades of the turbine rotor.

Some of the steel makes used for the casting of these parts are 1.4314 GX4CrNi13-4 or 1.4414GX3CrNiMo13-4 [1], [2]. The chemical compositions of the two types of steel are shown in tables 1 and 2 respectively:

C%	Si%	Mn%	P%	S%	Cr%	Mo%	Ni%
Max	Max	Max	Max	Max	12.00	Max	3.50
0.06	1.00	1.00	0.035	0.025	13.50	0.70	5.00

**Table 1.** Chemical composition of GX4CrNi13-4 (1.4313) steel.

	C%	Si%	Mn%	P%	S%	Cr%	Ni%	Mo
Min.	0	0	0	0	0	12.00	3.50	0.30
Max.	0.05	0.70	1.50	0.040	0.015	14.00	4.50	0.70

**Table 2.** Chemical composition of GX3CrNiMo 13-4 (1.4314) steel.

These two steel makes are used because they have a good resistance to corrosion, high tenacity and strength, as well as a high weldability. In order to optimise the casting technology we used the AnyCasting software allowing the researcher to elaborate several casting variants and to obtain a part closer to the performances expected in exploitation. These variants are obtained mainly by setting several casting parameters such as casting speed, filling rate, casting temperature, temperature of the casting mould, the meshing of the part and of the liquid pressure in the casting mould.

The objectives aimed at are: enhancing the efficiency of the mould and position of feeders, locating the casting defects, i.e. closed and open cavities, pores, fissures, air bubbles, and their directing to the areas decided by the designer by orienting the thermal flux; reducing the number of casting defects and decreasing the quantity of liquid metal. From the practical experience we may list over 70 casting defects specific to this type of part (different defects or defects of the same type, but of different sizes). These defects were found throughout the entire volume of the part. The distribution of defects is the following: in the upper area, in the central zone, in the zone of the block windows and in the lower section. The defects are open macro-cavities in the upper section of the block, technologic defects in the form of closed secondary cavities in the medium and inferior section of the part. The defects in the block's superior section are determined by the casting conditions and the inappropriate design of the mould and feeders. The closed secondary cavities in the middle and inferior section of the part are determined by the geometry of the part, as well as by the presence of thermal knots. The presence of the closed defects in the central and lower area does not allow a good equilibration of the block. Another type of defects are the micro-cavities, air bubbles and porosities found throughout the entire mass of the part, determined by the human factor. These defects occur because of the inadequate elaboration of steel, faulty deoxidation, insufficiently dried casting mould and paint at the beginning of casting. These aspects cannot be highlighted yet by the simulation software.

## 2. Presentation of the AnyCasting software

The experimental research was generally utilised in order to find the effect that the patterns, i.e. the filling and solidification types, have on the qualities of the product. Nevertheless, due to the specific features of the casting process, there are limits as regards its visualisation. Nowadays, the research for enhancing the casting process is performed both through experimental casting projects and by numerical simulation. Simulation may be very useful for the improvement of the initial project and for the validation of the modifications in the project, and it may provide information on the filling and solidification patterns even in the areas that are not visible, as they are covered by melt or mould, grace to the options of the software allowing the sectioning of the model in certain areas [3].

Based on this information, we may identify the problems occurring in the design of the manufacture process, making it possible to reduce costs and to increase productiveness.

The software is made of the following modules:

### 2.1. AnyDBASE

AnyDBASE is a database programme used for managing the properties of ferrous and non-ferrous alloys, of the properties of the moulds, paints, refractory materials used etc. that have to be selected in AnyPRE. AnyDBASE is conceived so that it may allow the accessing of two types of databases: the general database and the user database, the latter being utilised for modifying or adding materials. The general database contains the properties of ferrous, non-ferrous, non-metallic and functional alloys according to different international standards (KS, JIS, ASTM, etc.). In the user database we may create and manage a personally customised database.

### 2.2. AnyPRE

AnyPRE performs processing, by reading the CAD data, allows us to import the.stl extension files containing the part geometry and then turns them into.gsc files. The.gsc files store information related to the initial simulation data and allow the setting of simulation information in order to run it in anySOLVER. AnyPRE offers functions of network generation, generating networks with tens of millions of elements. We may also choose a variable meshing in certain areas of the part by using the variable mesh function of anyPRE. Moreover, it allows the selection of the processes and groups of working materials and the setting of heat, gating conditions etc. In conclusion, AnyPre creates three files, which determine the results of the simulation:

- project with the \*.gsc extension – it contains the data of the simulation used in anyPRE;
- project with the \*.msh extension – it contains information on the mesh networks;
- projects with the \*.prp extension – it comprises the simulation conditions.

### 2.3. AnySOLVER

AnySOLVER reads the input files from anyPRE and simulates the flowing and the temperature fields of the designed process. All aforementioned processes are calculated by a single solver.

### 2.4. AnyPOST

AnyPOST reads the results created in anySOLVER and shows the results graphically. anyPOST offers the opportunity to visualise the basic results such as: filling time, solidification time, outline (temperature, pressure, speed), the speed vectors in two or three dimensions, and creates plots based on the sensor results. We may also verify the various solidification defects in two or three dimensions using the combined results function.

## 3. Applications in AnyCasting

We shall proceed by presenting applications of simulations on the assembly of the cast rotor block part and the assembly of the turbine blade.

### 3.1. Applications in AnyCasting [4] on the set of the rotor block part

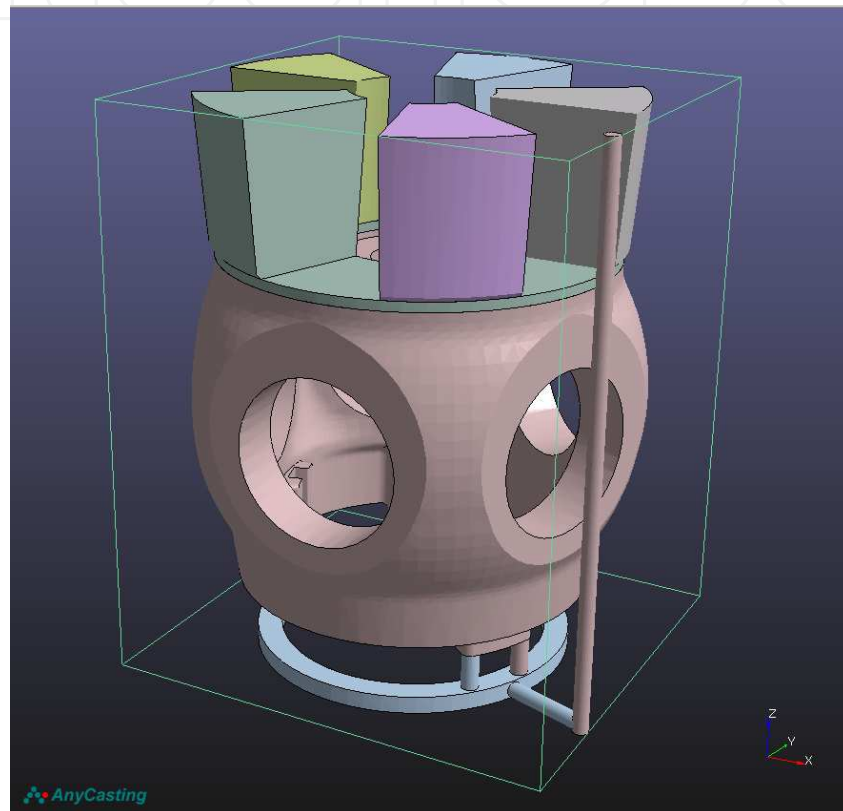
After the realisation of the solid in Solid Works, it is imported into AnyPre, where we introduce all the data necessary for simulation, the material being selected from AnyDBase [5] together with the physical-chemical properties. Four simulations were performed:

1. Simulation of the casting of the assembly of the rotor block part on the basis of a classic technology with single inferior feeding, without coolers and with feeders only in the upper section;
2. Simulation of the casting of the set of rotor block part with a technology using external coolers in the lower section of the block and feeding from a three-level casting network;
3. Simulation of the casting of the assembly of the rotor block part based on a technology with external coolers located in the lower section and under the area of feeders, and with exothermal powders;
4. Simulation of the assembly of the rotor block part with a technology using external coolers in the inferior section and under the feeders' zone, exothermal powders and feeder-covering powders, as well as blind feeders.

We chose the four variants in order to observe the influence of coolers and of blind feeders, as well as the evolution of casting defects in each variant, the influences that will define the type and position of defects.

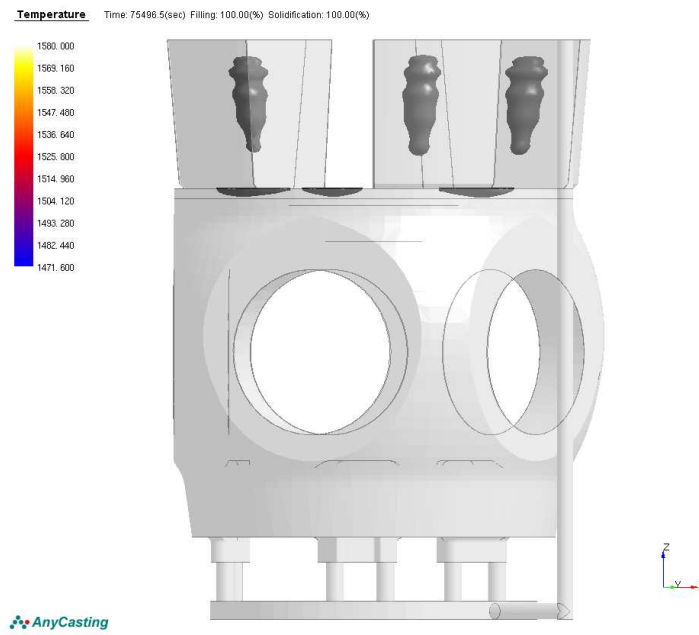
3.1.1. *Simulating the casting of the set of rotor block part with a classic technology with single feeding at the lower part, without coolers and with blind feeders situated only in the upper section*

Figure 1 presents the geometry of the block part corresponding to variant 1. The mould has a single feeding network by indirect casting from the lower part, technologic feeders being placed normally at the top. The mould is made of sand without coolers and no exothermal or insulating powders are used. The casting temperature is 1580°C, and the casting time is 240 seconds.



**Figure 1.** Geometry of the block assembly.

From the *set probabilistic defect parameter* menu we select the *defect parameter* criterion which presents the defect in the most accurate manner, and its position in the part volume. In the postprocessor we will see the results of simulation by types of defects, i.e. the macro-cavities located in the upper part of the casting assembly, that is in the area of feeders and in the upper section of the part, followed by the defects from the central area and those situated in the block inferior section. Figure 2 shows the position of the defects through the analysis of the *temperature variation* criterion during the filling and solidification of the cast set. The macro-defect under the form of open cavities is located in the superior part of the set and exceeds the joining area of the feeders with the body of the part [6]. Defects of this type are located on the surface of the part, may be seen with the naked eye and can be repaired by welding.



**Figure 2.** Position of macro-cavities in the block.

The same defect occurs also in Figure 3, the transparent visualising mode allows visualising the defects both from the viewpoint of position and from the perspective of mould and volume. We may also remark in Figure 3 that both defects are identical as regards position and shape with those in Figure 2. The analysis of this type of defects and the measures to be taken for their elimination were presented in detail in [6].

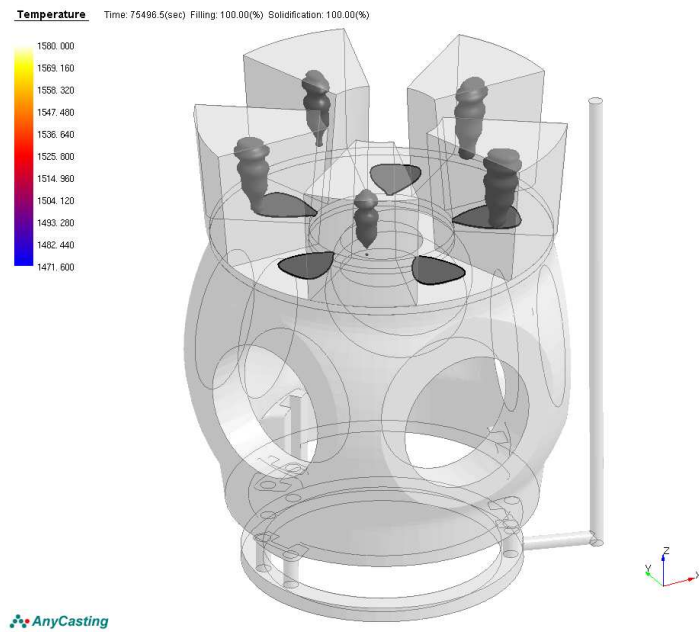


**Figure 3.** Position of macro-cavities in the block - 3D.

The defects taking the shape of closed secondary cavities in the middle area and in the lower section of the part are defects that cannot be observed by free visualisation and require non-destructive investigations, sometimes even by cutting the part for highlighting them. The presence of this type of defects makes it difficult to put the rotor block set into operation. These kinds of defects cannot be remedied and they generally trigger the discarding of the entire cast part. In Figure 4, section through the block, based on the *local solidification time* criterion, we see the variation of the solidification time in each zone, and the way in which each area of the casting assembly solidifies. We remark that the last zone to solidify is the area under the feeders and the lower zone of the part; between the block window and the feeding network. The alloy solidifies the fastest in the peripheral areas, from bottom to top, in the sense opposed to the casting direction, then the feeders' area. In the upper section of the part, under the feeder, thermal knots appear during solidification, determined by the modification of the part geometry, and the presence of these thermal knots indicates the occurrence of casting defects. From the analysis of solidification in the same Figure 4 we remark in section that in the central area (see the right zone) the prediction of the occurrence of other defects, presented in Figures 6 and 7.

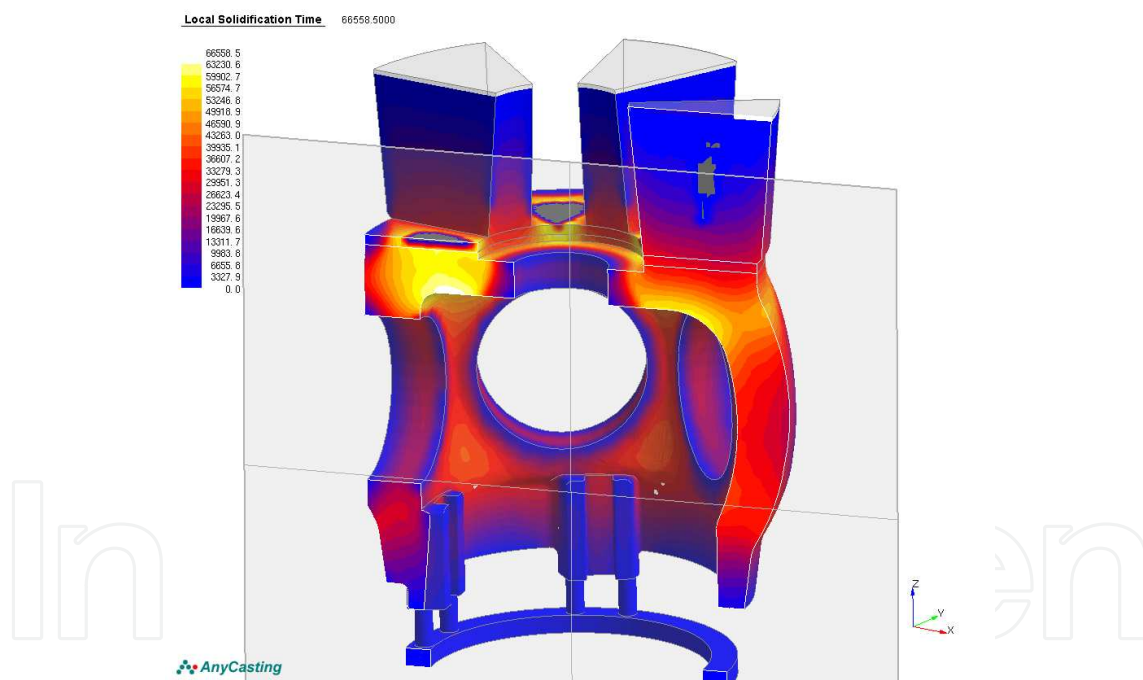
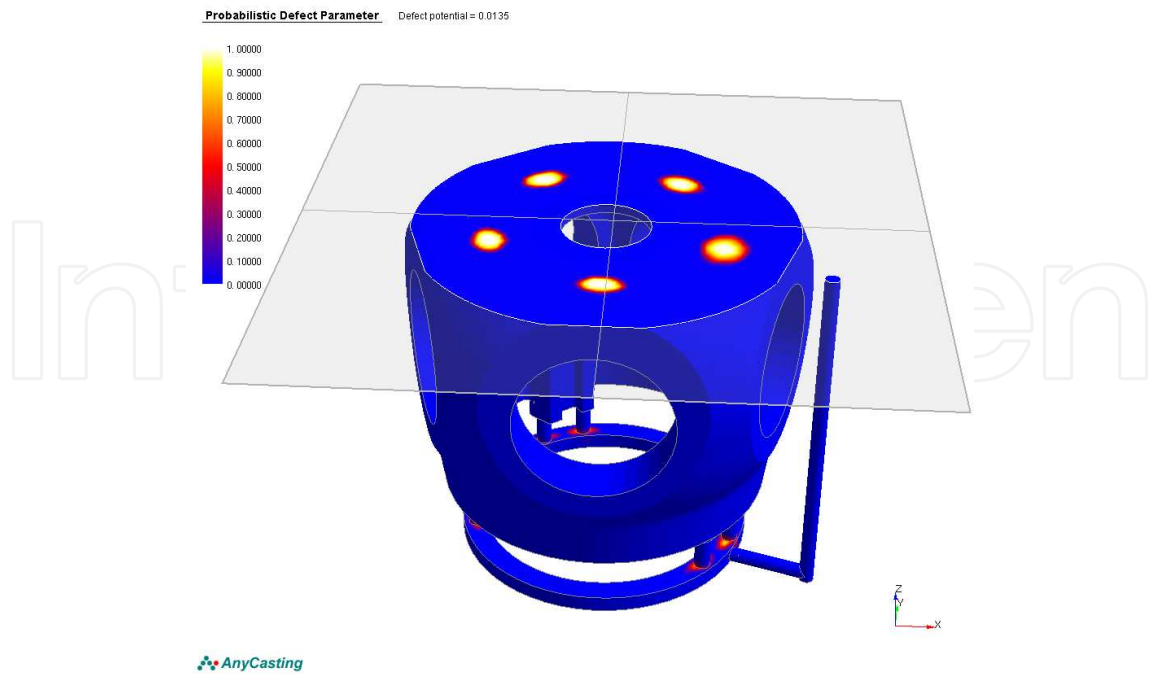


Figure 4. Local solidification time - section.

In Figure 5, by analysing the *defect parameter* probabilistic criterion, we observe the defects in the form of micro porosities and secondary or closed cavities in the part. The position of defects under the window in Figure 5 confirms the prediction of defects anticipated in Figures 3 and 4. From the analysis of the colour code bar, situated on the left side, in Figure 5, these defects' probability of occurrence in the area under the feeders has the maximum value 1,000, which means that the presence of these defects is inevitable.



**Figure 5.** Micro porosities and secondary cavities.

These defects are located under the feeders and reach the medium section of the part, Figure 6, in the windows area and in the lower section, Figure 7. The position and shape of defects is a confirmation of the prediction provided by the criterion presented in Figure 4.

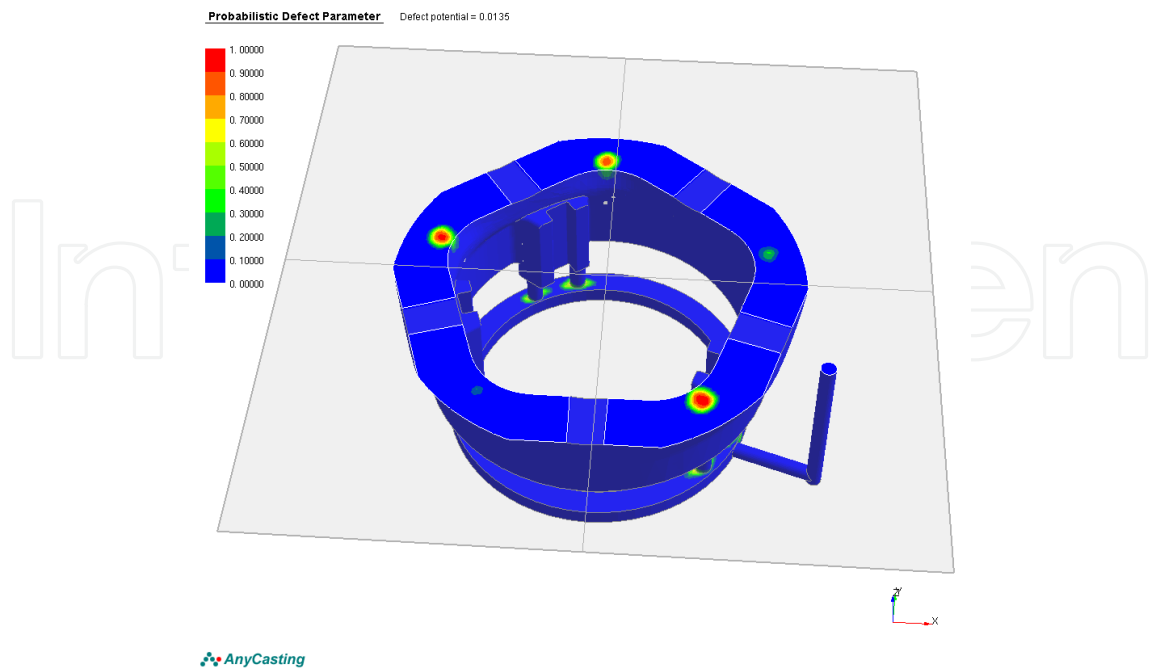


**Figure 6.** Micro porosities and secondary cavities.

Figure 6 confirms the presence of casting defects also in the lower section of the part, especially in the zone of the block windows. In this case too the probability of the apparition of defects is approximated based on the colour code displayed on the left side of the figure and it is estimated at 1,000 again. Figure 7 shows, by means of the criterion *variation of the temperature gradient during solidification*, the possibility of casting defect occurrence in the body of the part, i.e. in the superior and middle section, in the windows area and in the inferior side of the assembly.

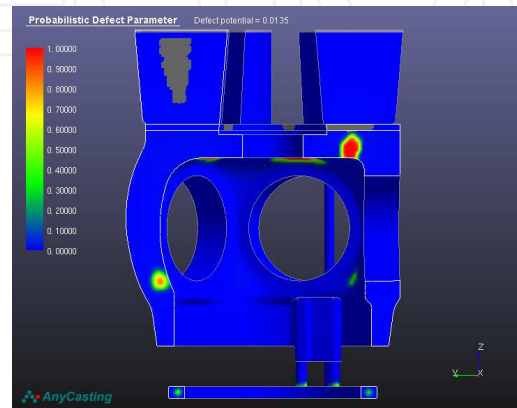


Figure 7. Temperature gradient.

In Figure 8, the *iso solid fraction curvature* criterion defines the position of defects in the middle zone, the windows zone and the lower section. In order to understand the criterion, we consider that the blue surfaces solidify the fastest; whereas the red surfaces are the slowest to solidify.

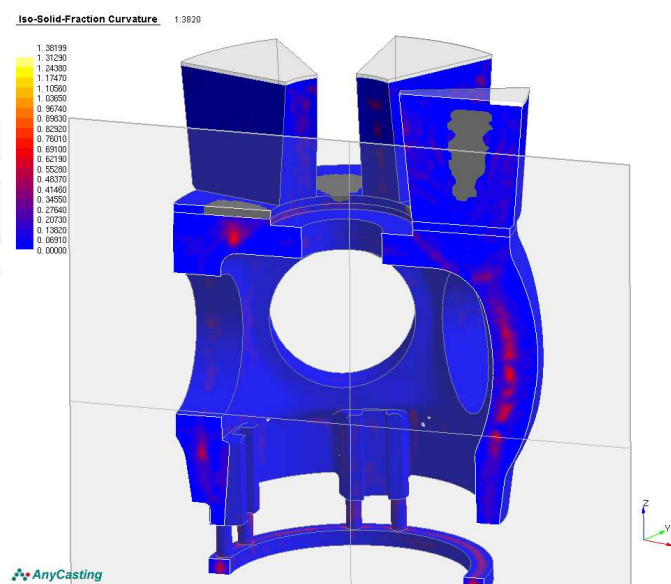
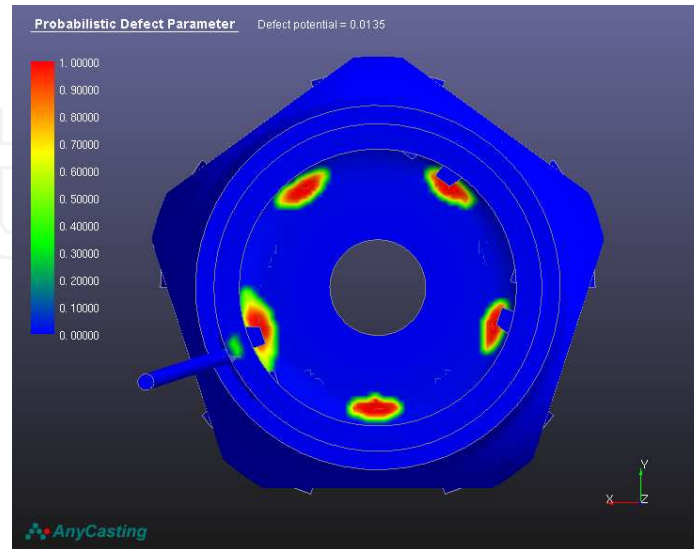


Figure 8. The *iso solid fraction curvature* criterion.

In Figure 9, highlighting micro porosities and secondary cavities, the defects in the window area are evident.



**Figure 9.** Micro porosities and secondary cavities.

#### 3.1.1.1. Partial conclusions

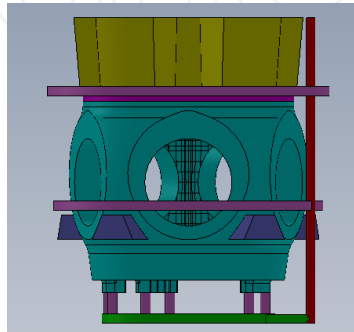
By simulation we highlighted the defects formed in the cast assembly, i.e. the open macro-cavities located in the upper section of the part, as well as other defects which may occur in the central area, the windows zone and the lower side of the part. The apparition of defects in the central and lower area is triggered by the part geometry.

The thermally narrowed areas produce cavities and porosities caused by the presence of the thermal knots. The elimination of defects due to the change of the part geometry is done by adding external coolers or by adding extra feeders. In order to avoid the formation of cool drops in the walls of the casting mould due to the high speed of the feeding jet, we shall choose a positioning of attacks so that they concentrate the thermal gradient towards the feeders. A possible measure for avoiding cool drops is feeding the casting mould in steps. The last attack level of the casting leg must be placed at the feeders' basis, in order to ensure the heat flow necessary to orient the thermal gradient towards the part's upper side.

#### 3.1.2. Simulating the casting of the assembly made of the rotor block part with a technology with external coolers on the block lower side and feeding with a three-level casting network

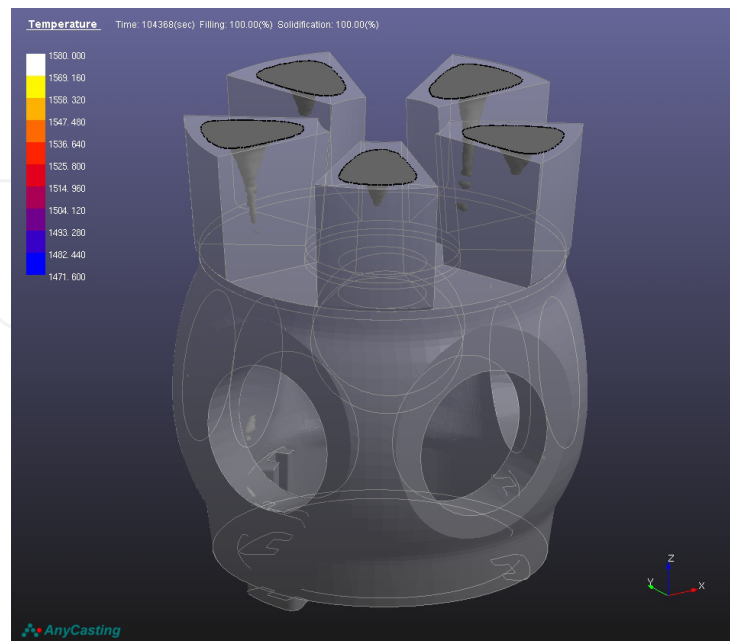
In the case of casting the rotor block set, which is a large part with the mass of approximately 12,000 kg, using only a liquid feeding in steps, we cannot totally control the orientation of the thermal gradient, and this is the reason why we use coolers. Coolers may be external coolers (their thickness should not exceed half of the thickness of the part wall in the application area) or internal soluble coolers.

The soluble internal coolers are very efficient, but much more difficult to control. For an efficient use the coolers must be heated before use to a temperature of around 80°C, in order to avoid the boiling of the jet of liquid metal in contact with them. The use of cold coolers risks triggering violent reactions, leading to the erosion of the mould in the respective area and the occurrence of vortices which trigger the oxidation of the liquid, with negative influences on the part quality. Figure 10 presents the geometry of the rotor block casting set corresponding to the casting variant 2.



**Figure 10.** Block shape.

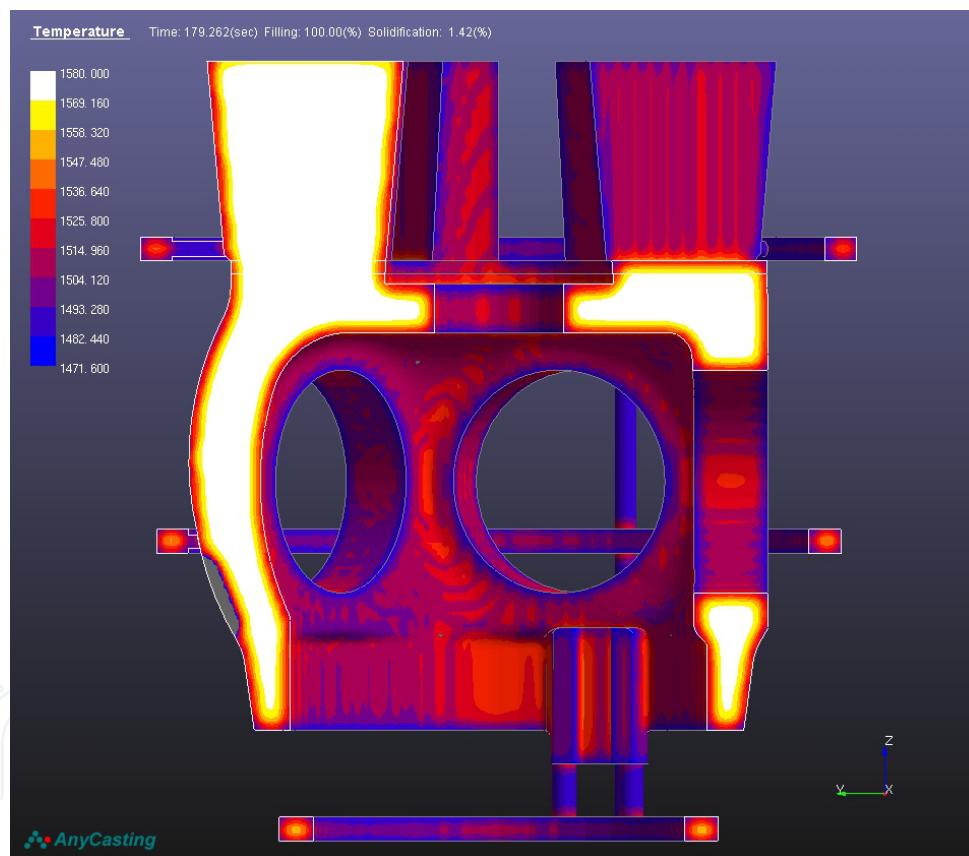
In this variant, the part is fed by a three-step casting network for a feeding meant to avoid the formation of cold drops or oxides in the part, and external coolers for directing the thermal gradient towards the areas intended by the designer. Figure 11 shows the cavities occurring in the upper section of the casting set.



**Figure 11.** Cavity porosity - 3D.

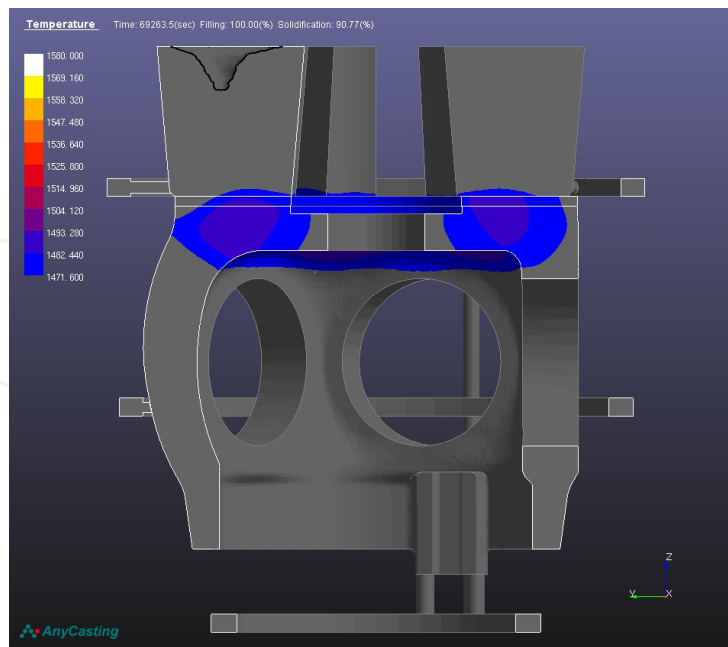
The transparent display mode allows the visualisation of the defects throughout the entire volume of the cast assembly after solidification ends and the temperature in the mould is much below the steel solidus temperature. Moreover, in the light grey areas located in the lower side of the block windows we remark the presence of local cavities defects. Defects of this type were present also in the casting variant 1. The absence of defects in the lower zone, under the block windows, indicates that the external cooler manifests its effect by the fact that solidification in the respective zone takes place during the mould filling.

In Figure 12, grace to the *solidification temperature* criterion, we can follow the temperature variation during solidification at 100% filling and the beginning of solidification. In the lower left side we remark the effect of the cooler by the fact that the crust temperature is lower than the temperature in other zones of the assembly.



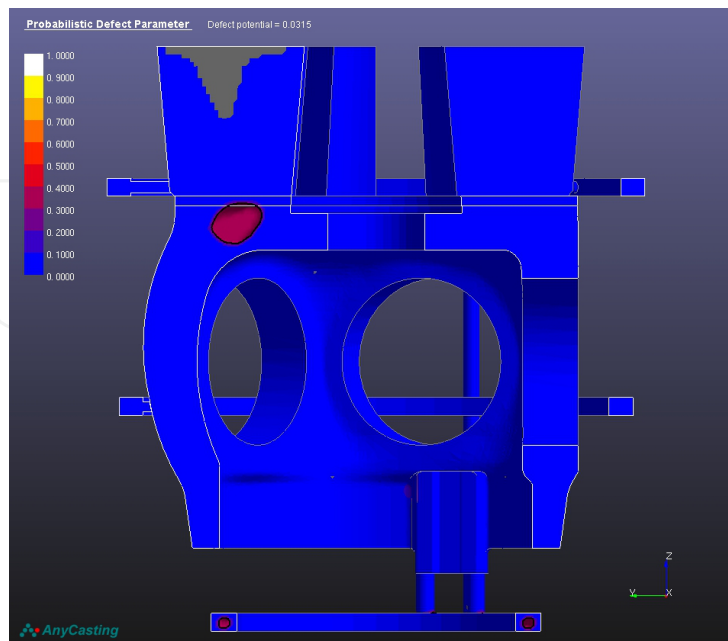
**Figure 12.** Solidification temperature - at 14% solidification.

Figure 13 presents, also through the *solidification temperature* criterion, the temperature variation during solidification at 100% filling and solidification completed in proportion of 90.7%. We can see that the casting defects are located in the feeders and in the zone under the feeders towards the lower section of the part. The temperature in the coloured zones is still higher than the solidus temperature, which proves that these areas are the last to solidify.



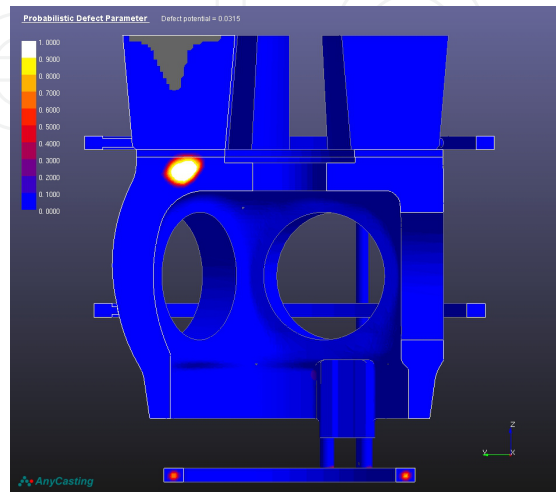
**Figure 13.** Solidification temperature - at 90% solidification.

Figure 14, through the *solidification temperature* criterion - 14% solidification, shows the position of the defect at the beginning of solidification. In the dark red zone a casting defect will occur under the form of a secondary cavity. In this phase the occurrence probability ranges between 0.300 and 0.400. The colour analysis is done based on the colour bar displayed on the left side of the figure. Like in the previous case, this zone will solidify the last.



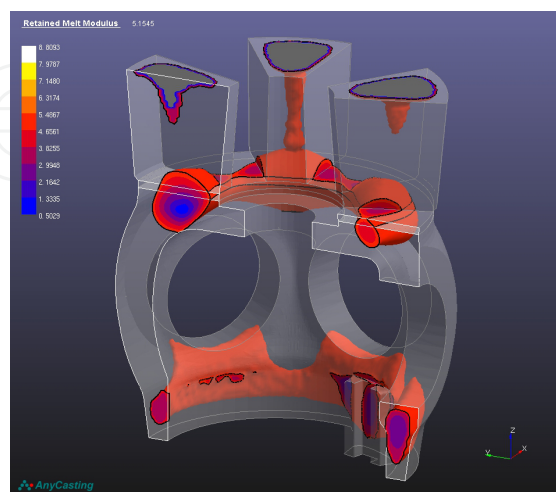
**Figure 14.** Retained melt volume - 14% solidification.

Figure 15, still through the *solidification temperature* criterion at the end of solidification confirms the fact that the casting defect will be located under the feeders, in the upper zone of the part, and the probability of its occurrence in this case is of 0.400 on a scale with the maximal value 1.000. The analysis is performed also with the help of the colour bars displayed on the left side of the figure, the colour of the area being whitish.



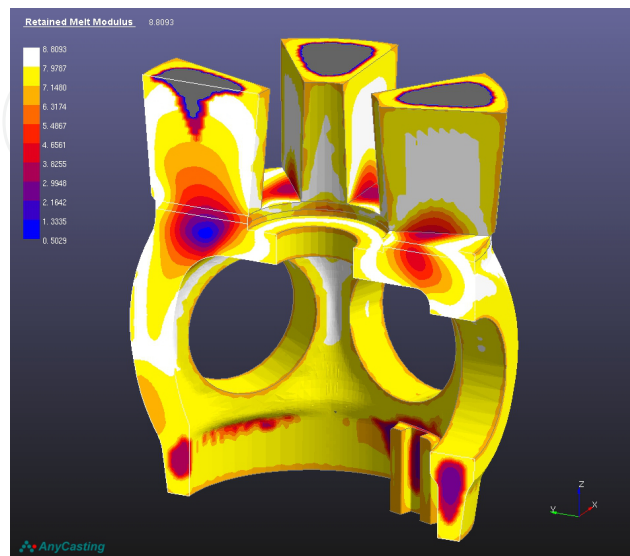
**Figure 15.** Retained melt volume - 90% solidification.

Figure 16, by the analysis of the *retained melt modulus* criterion at the start of solidification, shows an overall image of the cast part solidification along time. This figure presents the heat-influenced areas in different colours. The defects are already occurring in the superior part, in the feeders, under the feeders towards the central zone of the part. At the part lower end, the coloured area under the windows starts to solidify more rapidly, and the position of the defect is already anticipated in the upper side of the part.



**Figure 16.** Retained melt modulus - 14% solidification.

In Figure 17 we can see the efficiency of the cooler in the lower part in the yellow areas; the defect appears under the windows and in the windows zone. Figure 17 clearly shows the part of liquid separated in the lower section and not compensated by re-feeding with liquid metal. In this figure also the defects in the block window are highlighted in white.



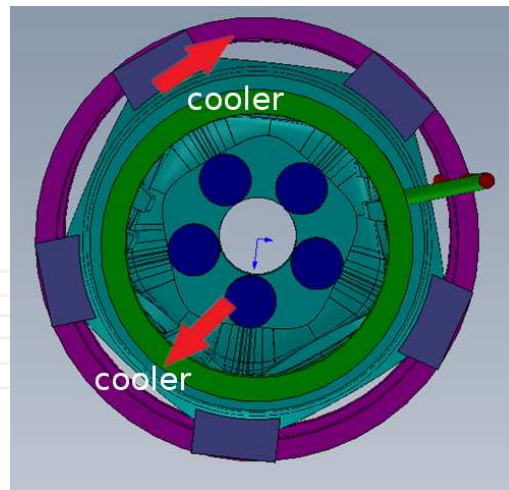
**Figure 17.** Retained melt modulus - 90% solidification.

### 3.1.2.1. *Partial conclusions*

In this simulation variant we remark the influence of the cooler by the fact that defects in the lower side of the part disappear. The part is fed by means of a three-step casting network destined to avoid the formation of cool drops or of oxides in the part. The external coolers determine the directing of the thermal gradient towards the zones chosen by the designer. However, they do not solve the problems entirely.

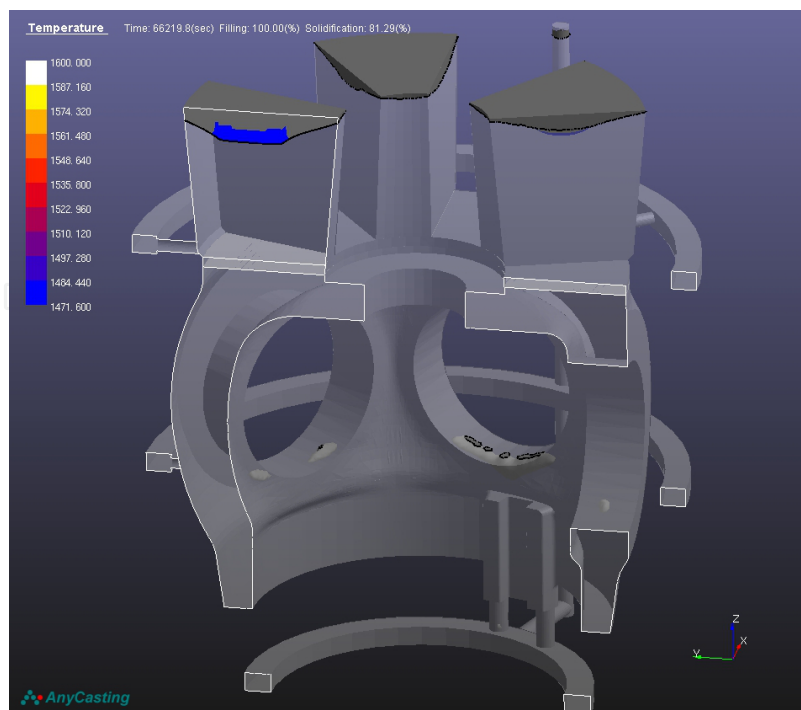
### 3.1.3. *Simulating the casting of the rotor block part assembly using a technology with external coolers in the lower section and under the feeders area, as well as exothermal powders*

It is less economical, but nevertheless very efficient, to use exothermal mixtures such as plates, bushes, exothermal powders, izolex or pearlite insulating powders. Besides these we may also utilise covering unguent powders in order to facilitate the liquid flow along the mould walls, and at the same time in order to compensate the heat losses in the upper side of the cast part, which leads to a longer heat preservation in feeders, gradually reaching an accentuated temperature gap between the upper and lower sections of the cast part (with influence on the thermal gradient). In this example, we present the casting simulation applied to the rotor block part using three-step feeding and external coolers in the lower side of the part, under the feeders' area, and exothermal and insulating materials in the upper side of the part, as shown in Figure 18. The simulation respects the same conditions regarding the physical-chemical properties of the liquid, but makes the aforementioned technological changes.



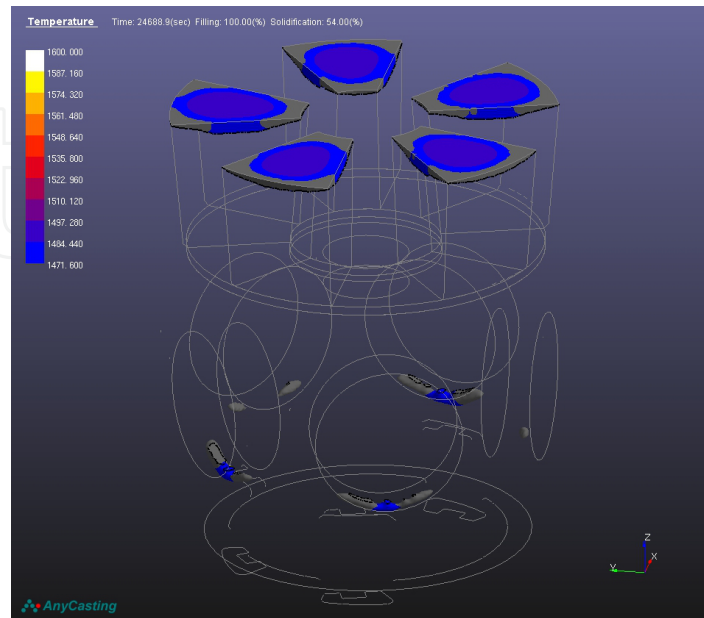
**Figure 18.** Casting mould equipped with coolers.

This approach solves the problem of cavities under the feeders, but the defects analysed in the casting variants 1 were not eliminated. Figure 19 shows in section the position of cavity and porosities; the open cavity macro-defect is present in the upper side of the feeder, whereas the porosity defect occurs in the lower side of the rotor block window. Figure 19 also presents the depth reached by the defect in the part volume and at the same time we can see the effect of insulating powders, as the cavity volume is smaller than in the previous cases. We can see as well the defects in the block windows.



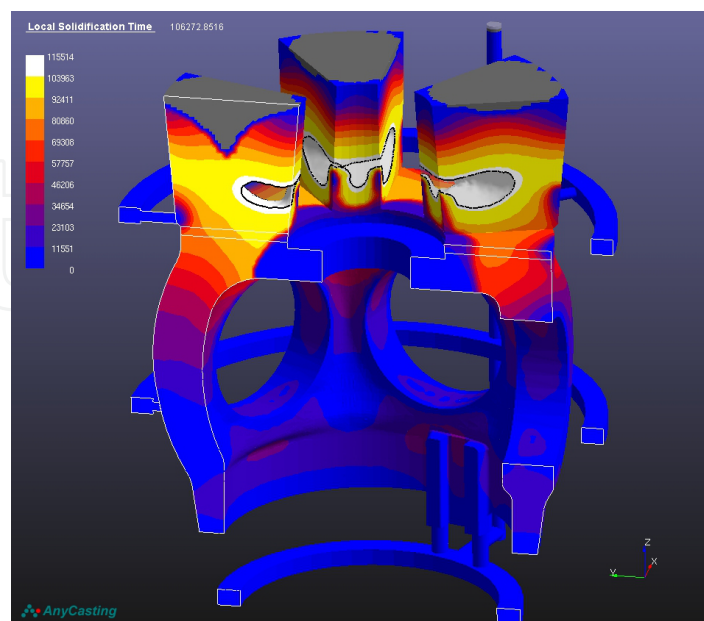
**Figure 19.** Position of cavity and porosities - section.

The same defect types are highlighted in Figure 20 too, along with all the defects appeared in the block window. The blue zones indicate the volume of these defects too.



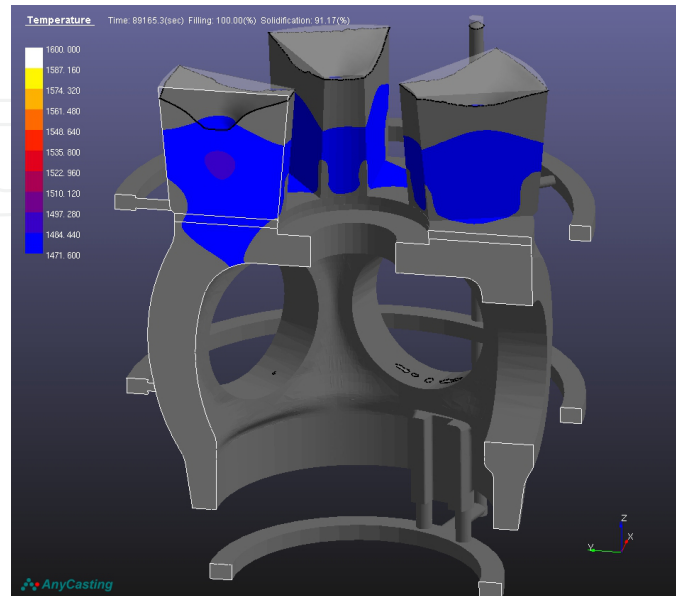
**Figure 20.** Position of cavity and porosities - transparent.

Figure 21 shows the evolution of casting defects depending on the local solidification time, in fact the solidification duration of each part zone is shown in section. We remark that defects are concentrated in the upper area of the feeder and in the window area.



**Figure 21.** Local solidification time.

In Figure 22, by the temperature variation during solidification and the evolution of defects during the solidification of the cast set, we remark that the defects have the same positions as in the previous figure.



**Figure 22.** Temperature solidification.

In Figures 23 and 24, we point out the influence of the *defect parameter* probabilistic criterion in accordance with the cooling rate and the *retained melt modulus* criterion, indicating at the same time that the defect occurrence probability is maximal in the light-coloured areas.

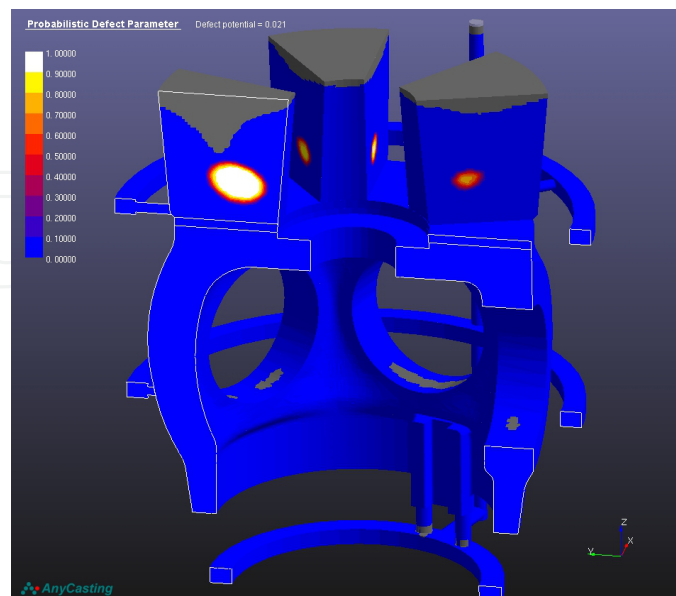


**Figure 23.** Cooling rate.

Figure 24, by means of the *retained melt modulus* criterion, identifies the defect formation probability based on the colour bar displayed on the left as being maximal in the technological feeders. We can see in light grey the cavities in the windows zone.

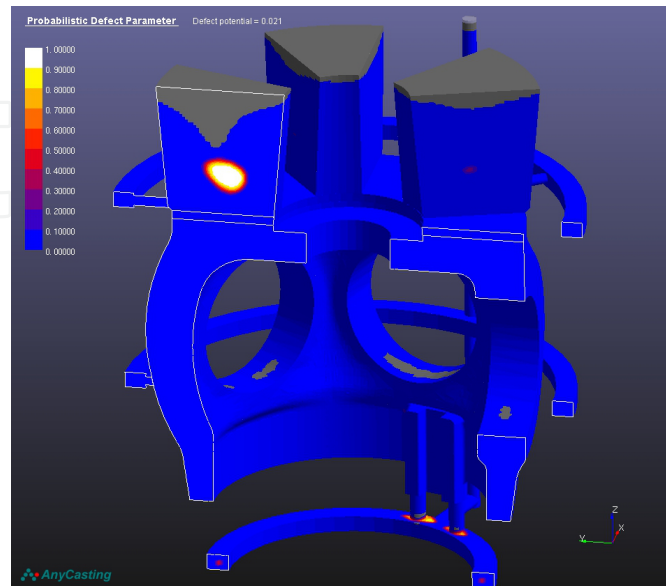


**Figure 24.** Retained melt modulus.

As a final measure for obtaining a defect-free cast part with all the sufficiency conditions fulfilled, we use in addition blind feeders and exothermal and insulating powders.

#### 3.1.3.1. *Partial conclusions*

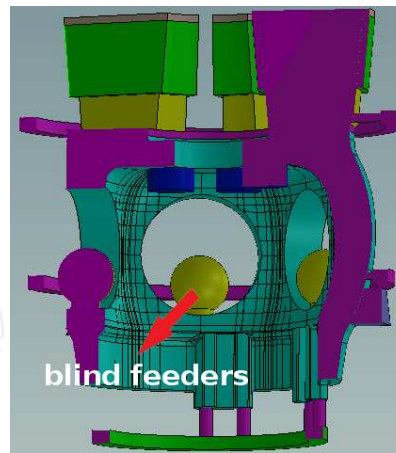
The presence of coolers in the lower and upper sides determines the gradient shift towards the superior side, which results in the elimination of defects in the lower side.

The utilisation of exothermal and covering powders leads to the reduction of the cavity in the area under the feeders towards the upper side of the part. The defects in the zone of the block windows remain still apparent.

#### 3.1.4. *Simulating the casting of the rotor block assembly part with a technology using external coolers in the lower section and under the feeders' area, exothermal and feeder-covering powders, as well as blind feeders*

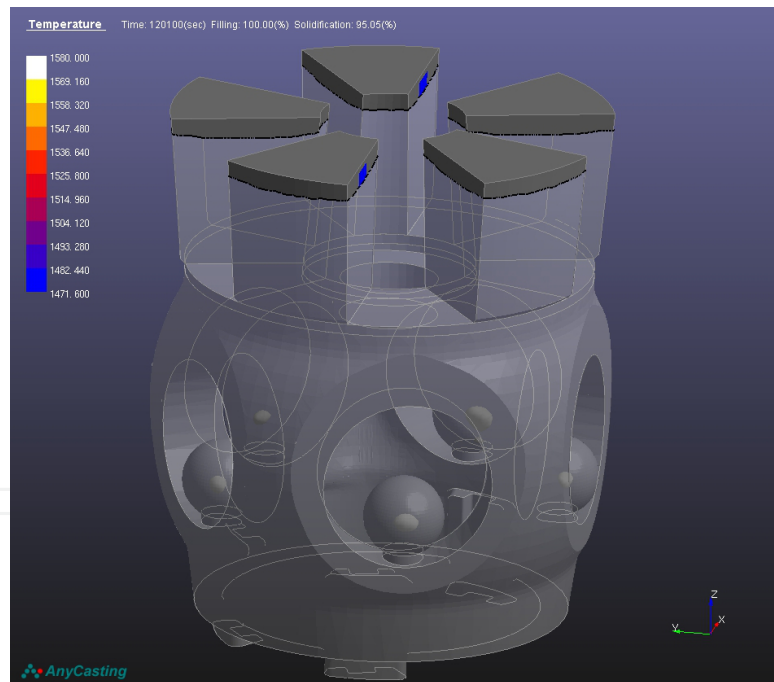
Figure 25 presents the casting assembly equipped with coolers and blind feeders.

In this variant we use external coolers in the upper side of the set, external coolers in the contact area between the feeders and the body of the part, and additional blind feeders in the windows zones as well as covering and exothermal powders. This variant, although more expensive, determines the reduction of casting defects, eliminating especially the interior defects, either in the middle or lower section.



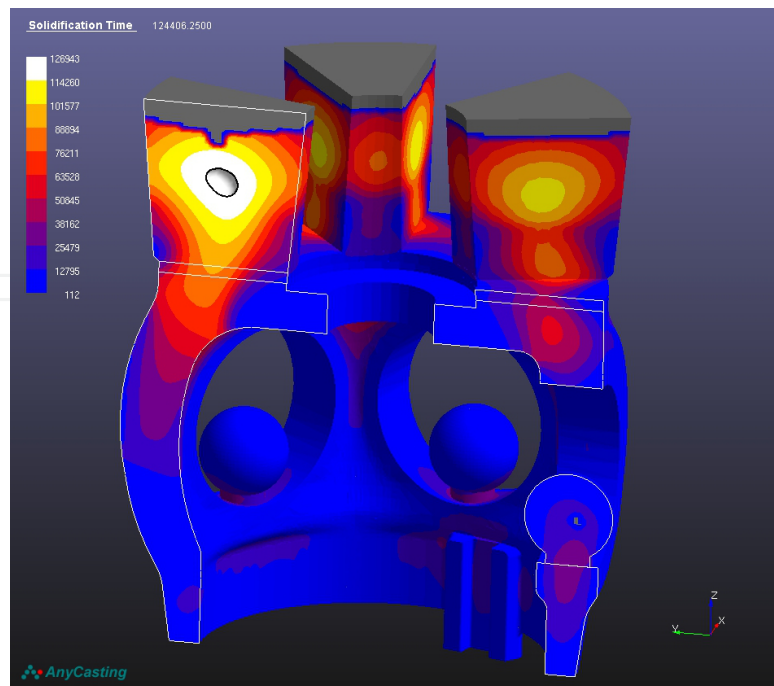
**Figure 25.** Casting mould equipped with coolers and blind feeders.

Figure 26 presents the position of cavities and porosities, the macro-defects in the upper side of the part and the superior section porosities located in the blind feeders, eliminating the defects in the windows zone.



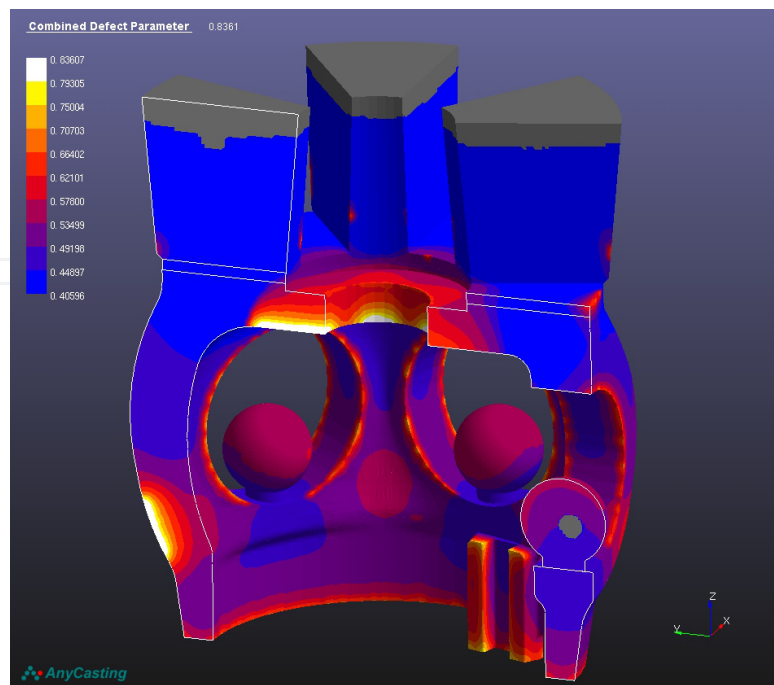
**Figure 26.** Position of cavities and porosities.

In Figure 27, grace to the *time solidification variation* criterion, we can anticipate the position of defects at the end of solidification, these defects being located in the upper side of the part and in the blind feeders. The efficiency of the exothermal and insulating powders is obvious by the fact that the macro-cavity in the superior side is smaller in volume than in casting variants 1 and 2. The block windows remain free from cavity defects.



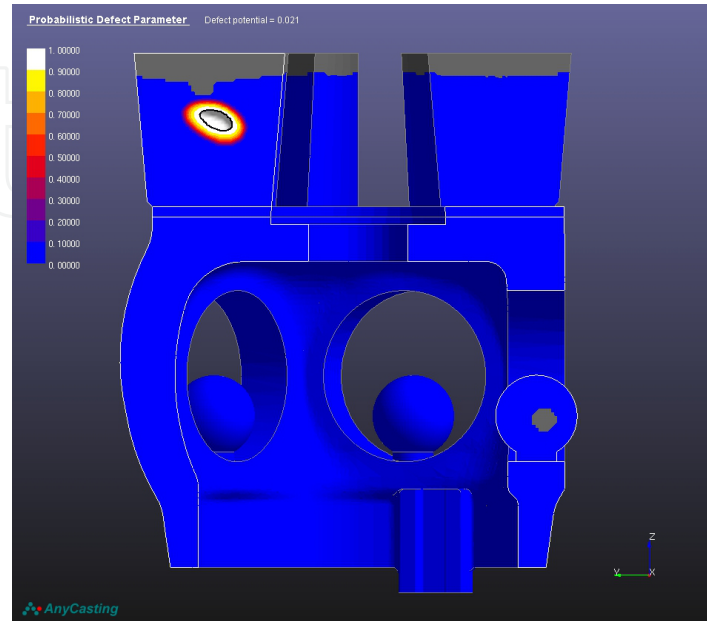
**Figure 27.** Solidification time.

Figure 28, through the analysis of the *cooling rate* criterion, presents the way in which the part solidifies, and accordingly the blue areas solidify the slowliest whereas the light-coloured zones solidify the quickest due to the effect of the added external coolers.



**Figure 28.** Cooling rate.

Still on the basis of this criterion we remark the effect of exothermal and insulating powders in the upper part of feeders. In both cases there are no defects occurring in the windows zone, the cavities being concentrated in the blind feeders.



**Figure 29.** Retained melt volume.

In Figure 29, based on the analysis of the *retained melt volume* criterion, we see very clearly the positioning of casting defects in the upper part of the external feeder, and in grey we identify the positioning of cavity defects in the blind feeder. The defect in the window area was shifted by the thermal gradient, i.e. by the modification of the solidification conditions, towards the centre of the blind feeder. All criteria used at this point indicate a healthy part without major defects.

#### 3.1.4.1. Partial conclusions

In this variant, the casting defects, grace to the directing of the thermal gradient, are eliminated from the body of the part and transferred to the feeders in the upper section of the part, whereas the defects from the windows zone are directed into the blind feeders.

#### 3.1.5. Practical results of the casting of the rotor block assembly part

We continue by presenting the practical results of the casting of the rotor block set part. The casting was performed using the results of the simulation in the first variant. After the verification of the cast part, the following resulted: the internal defects under the form of closed secondary cavities in the middle areas and the lower section were highlighted only by non-destructive investigation methods. Figure 30 shows the open defects (porosities) occurred in the lower area of the rotor block window. These defects are small in size and are located on the surface of the part, being apparent by direct visualisation.



**Figure 30.** Casting defects in the block window.

In Figure 31, porosity-type casting defects occur again in the zone of the rotor block window. The rotor block window open porosities do not occur in all windows. On the exterior surface of the part porosities are visible. The porosities on the exterior surface are due to the mould and paint insufficiently dried before casting. In Figure 31 we can also remark that the superior side of the block after mechanical processing is irregular due to the presence of macro-cavities casting defects. All defects presented in Figures 30 and 31 can be repaired by welding.



**Figure 31.** Porosity-type casting defects in the block window and on the exterior surface.

Figures 32 and 33 present the part cast according to simulation variant 4. We can remark in the two figures, by direct visualisation, that the upper side of the part; i.e. the feeders' zone, is very healthy and does not exhibit any traces of cavities inside the part, nor does it show other types of defects or porosities.

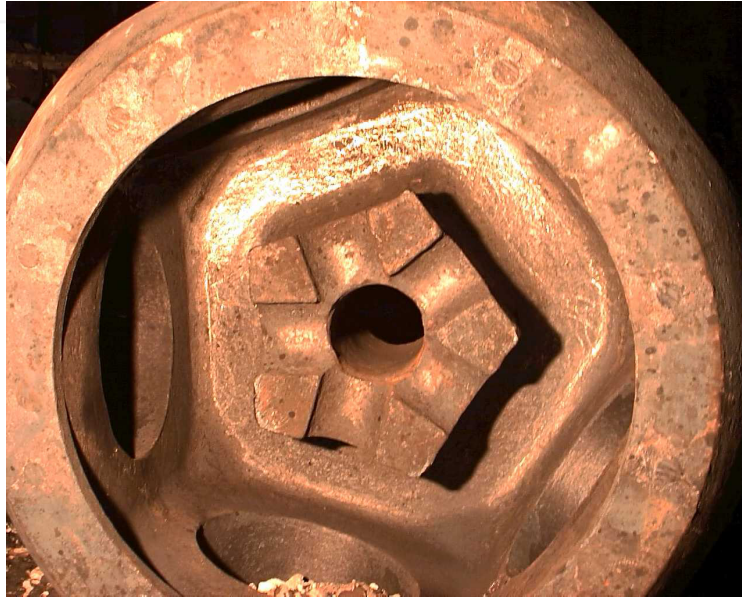


**Figure 32.** View of the rotor block upper side.

Similarly to Figure 33, the part is clean and free of casting defects visible on the surface of the part. On the part's exterior surface we can identify the traces of the mould casting network.



**Figure 33.** Overall view of the rotor block.

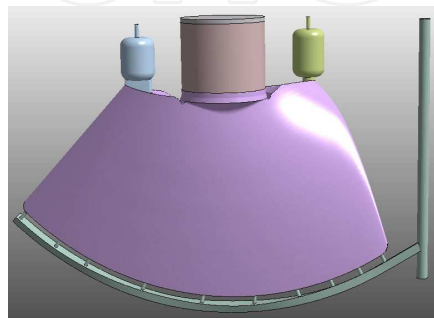
### 3.2. Conclusions

After having compared the results obtained by simulation with the results obtained by actually casting the part, we came up with the following conclusions:

- the most efficient casting variant proved to be the casting according to the simulation for the rotor block assembly casting using the technology with external coolers in the lower zone and under the feeders, exothermal and feeder-covering powders, as well as blind feeders, in the sense that this variant provokes the less defects;
- the information about the type of casting defects occurred in the rotor block assembly and the blades, and about the casting technologies for these complex parts are very scarce and not thoroughly treated in the literature.
- the contribution of simulation is obvious, due to the fact that we can highlight defects classified in defect catalogues that are updated rather rarely, at long intervals of time that can even exceed 50 years.
- the selection of simulation parameters may lead to less expensive solutions and to manufacturing higher quality parts.

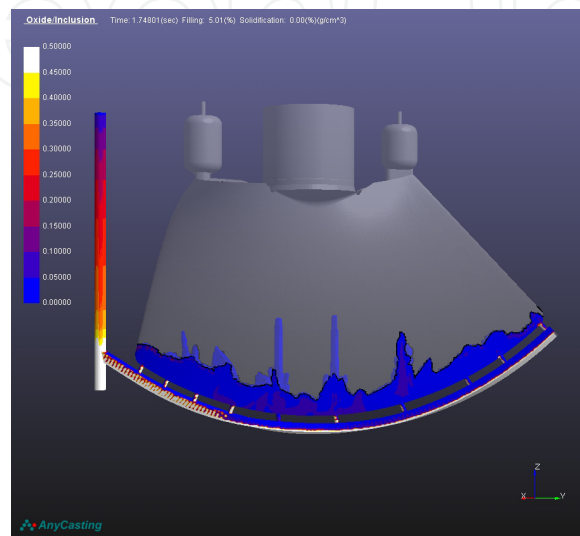
### 4. Applications in AnyCasting on the casting of the Kaplan blade part assembly

The chemical composition of the steels used in casting the blades are shown in Tables 1 and 2. The objectives to reach by simulation refer to obtaining a blade reliable in charge, with a low number of defects and water-resistant. After elaborating the geometry of the part in Solid Works a file is generated with the extension \*.stl. This file is imported into AnyPre, where we introduce all the data necessary for simulation, the material being selected from AnyDBase together with the physical-chemical properties. Figure 34 presents the geometry of the ensemble of blade part and the casting position. We designed a system of indirect casting with inferior liquid feeding and distribution by several feeders. In the upper side the casting mould is equipped with 2 feeders for the retention of gases and oxides formed during the mould filling. The mould is made of sand, the casting temperature being 1580°C.



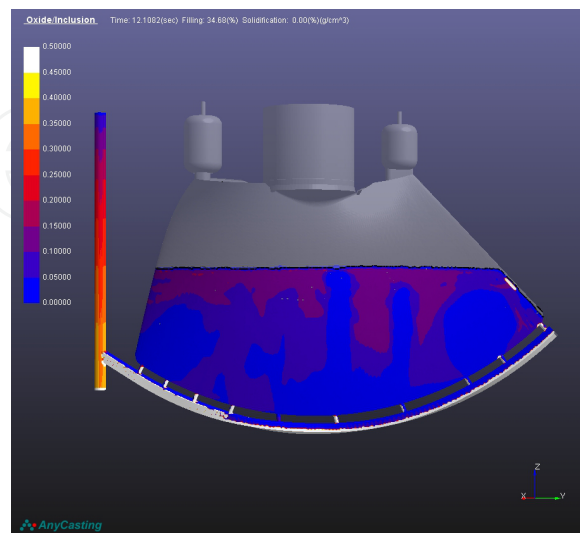
**Figure 34.** Geometry of the blade part assembly.

The most frequently encountered defects in the case of the blade casting are porosities, air bubbles and oxides, which appear on the surface. Specialists generally grant more attention to the solidification process to the detriment of the mould filling phases. In this case we shall especially analyse the mould-filling manner based on the *oxide inclusion* criterion. In Figure 35 we can see the penetration of the liquid alloy jet into the mould at 5% filling from the volume of the mould.



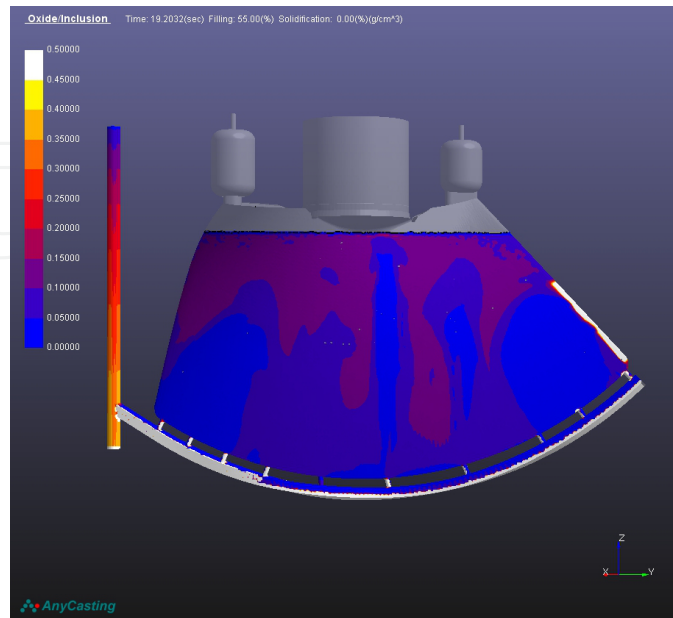
**Figure 35.** Oxide inclusion - 5.1% filling.

At the entry into the mould through the ingate the jet has a high speed due to the ferro-static pressure in the casting system. In figure 36 the jet of liquid metal is much calmer due to the counter pressure exercised by the quantity of liquid already existing in the mould.



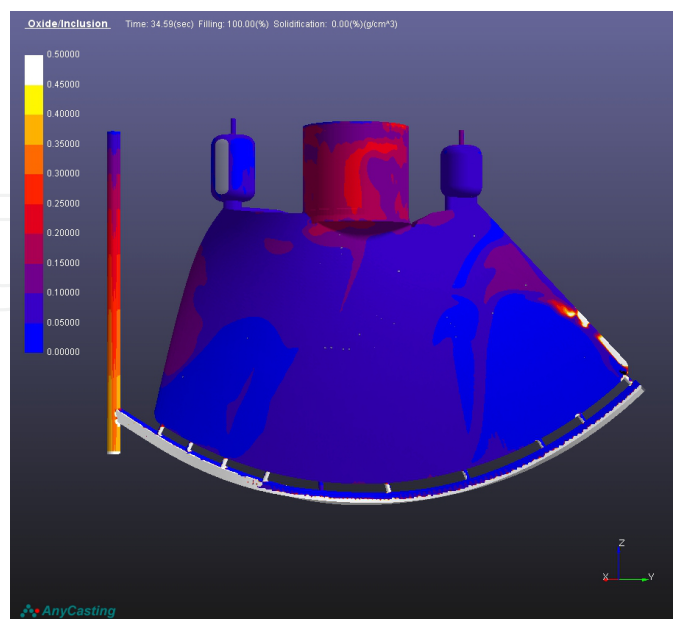
**Figure 36.** Oxide inclusion - 34% filling.

Figure 36 also shows that when we have filled 34% of the mould volume the oxides are raised together with the movement of the liquid in the mould.



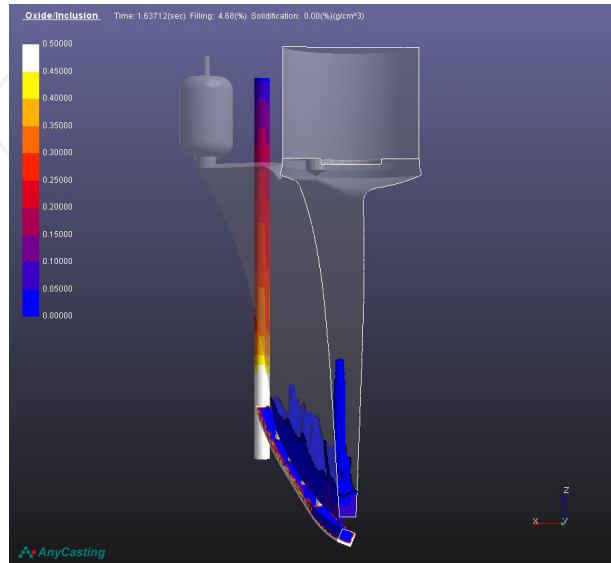
**Figure 37.** Oxide inclusion - 55% filling.

In Figure 37, with the help of oxide inclusion at a filling of 55% from the mould volume and in Figure 38, grace to the *oxide inclusion 100%* criterion, we have already defined the position of oxides and inclusions on the blade surface.



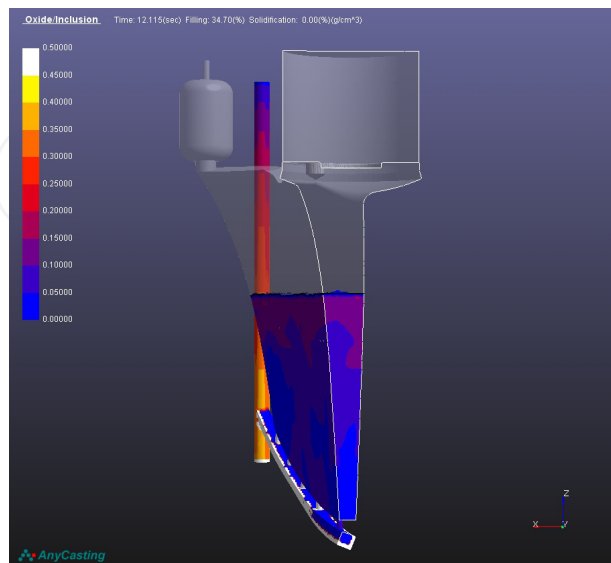
**Figure 38.** Oxide inclusion -100% filling.

The highest concentration of porosities is found on the active surface of the blade, towards its extremities in the lower, middle and upper sections. Figures 39 and 40 present the same phenomenon, this time in the section of the blade. We proceeded to the blade sectioning in order to observe if porosities are present also inside the blade.



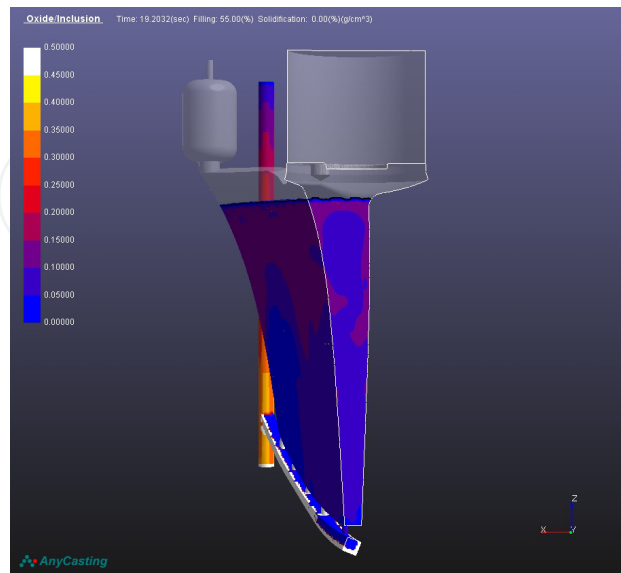
**Figure 39.** Oxide inclusion - 5.1% filling - vertical section.

Still in Figure 39 we observe the jet entering the sectioned mould, and we see that the central area has the highest speed, phenomenon apparent also in Figure 35. Figure 40 shows that the liquid jet feeding the mould exhibits oxides on the contact surface with the atmosphere from the mould.



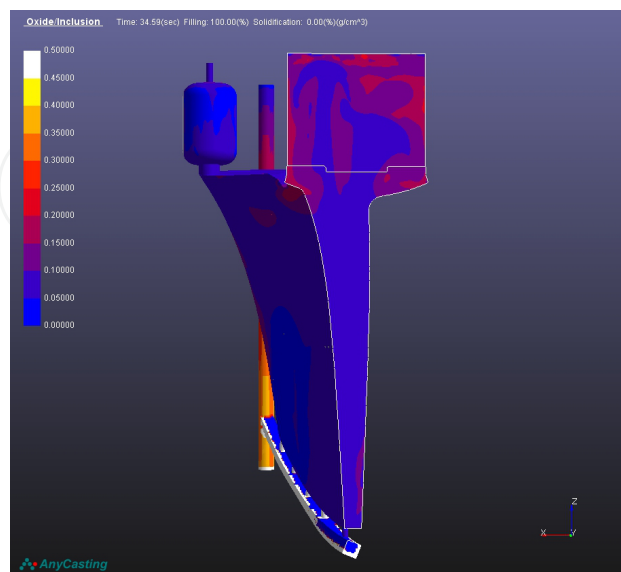
**Figure 40.** Oxide inclusion - 34% filling - vertical section.

Figures 39-42 illustrate the same criterion, this time in section. This mode of presentation enables the visualisation of the metal flow in the mould, a very important aspect for manufacturing defect-free parts and assemblies.



**Figure 41.** Oxide inclusion - 55% filling - vertical section.

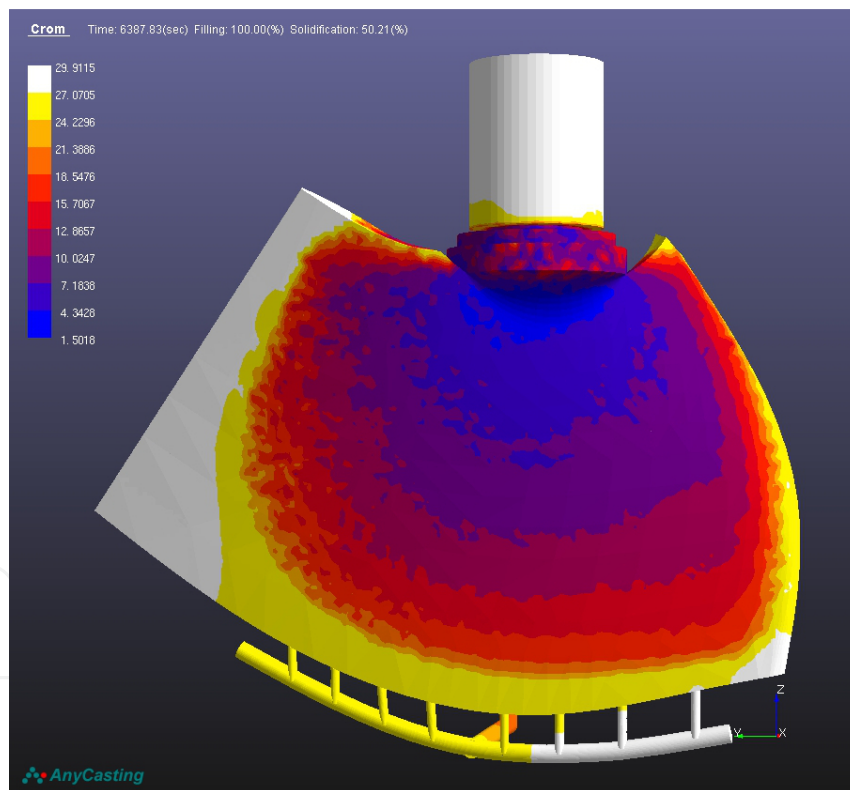
The oxidation reactions are powerful due to the high temperature of the jet and favoured if the mould is insufficiently dry so that it is free from interior moist. The drying is performed before casting in order to avoid the apparition of bubbles and porosities caused by the gases in the mould. A parameter that is not taken into account in simulation or in the real conditions is the air quantity driven by the metal jet into the casting network. Figure 41 showing the situation at 55% filling, and Figure 42 exhibiting the oxide inclusion at 100% filling define the final position of oxides, bubbles and porosities in the blade.



**Figure 42.** Oxide inclusion - 100% filling - vertical section.

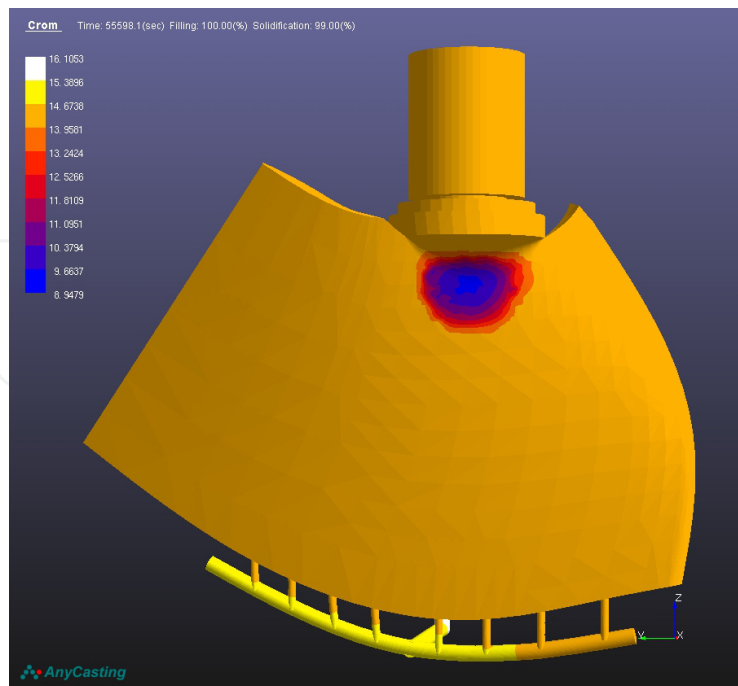
An important cause determining the occurrence of porosities and air bubbles is the failure to observe the technology of steel elaboration and deoxidisation. Another criterion affecting the quality of the cast parts is determined by the chromium segregation. Chromium has a high affinity to carbon and forms chromium carbides located in the volume of the part.

In Figure 43, showing the chromium segregation at 50% solidification, we can observe the areas where chromium segregates under the form of carbides. The zone where the segregation is the most apparent according the colour code bar is situated on the exterior sides of the blade and in its upper section, the maximum concentration being 29%. Segregation evolves in time so that at the end of solidification, according to Figure 43 showing the chromium segregation at 100% solidification, chromium is found throughout the volume of the blade at an average concentration of 15%. The chromium concentration in the change zone of the upper section, i.e. between the blade flange and the blade block, has the value 8.9% Cr (see the blue zone, Figures 44 and 46).



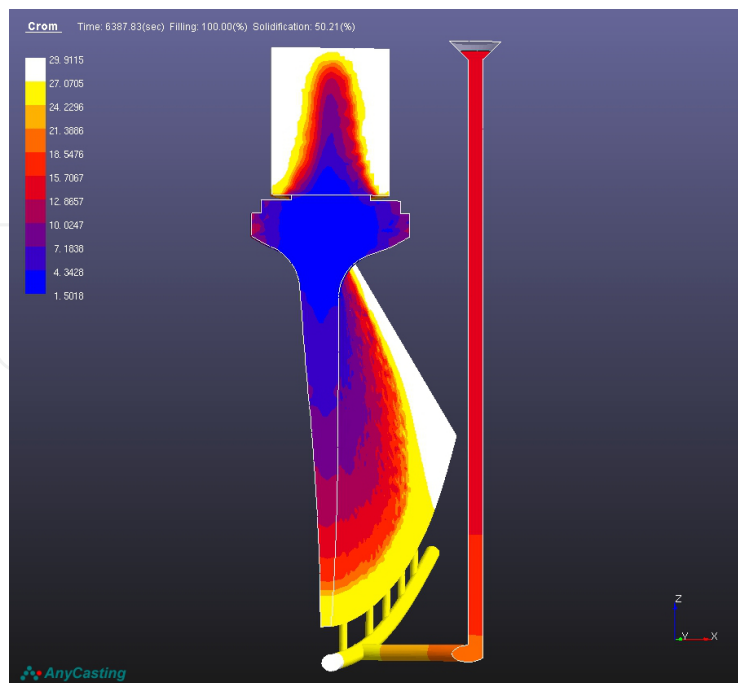
**Figure 43.** Chromium segregation at 50% solidification.

Figure 44 exhibits in frontal view the distribution of the chromium content on the blade surface, the area with the lowest chromium being the passage zone between the blade flange and the blade block.



**Figure 44.** Chromium segregation at 100% solidification.

The same chromium distribution is found also in Figure 45 highlighting the chromium segregation at 50% solidification in section, and in Figure 46, presenting the chromium segregation at 100% solidification in section.



**Figure 45.** Chromium segregation at 50% solidification - vertical section.

In Figure 45, in section, we remark that the zones with the maximum chromium content are highlighted in white, while the areas with minimum chromium content appear in blue. According to the colour bar, we can determine the chromium content in each section of the blade. Similarly, Figure 46 in section shows the distribution of the chromium concentration throughout the entire volume of the blade at the end of solidification.

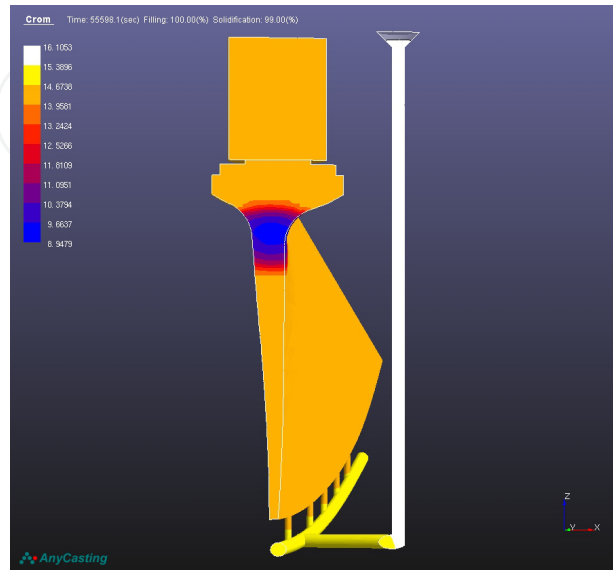


**Figure 46.** Chromium segregation at 100% solidification - vertical section.

Carbon has a high solubility in liquid state, the last part separating from the solution has a higher carbon content compared to the rest of the basic metal mass, which is iron. Figure 47 (carbon segregation at 50% solidification) and Figure 48 (carbon segregation at 100% solidification) reflect the carbon concentrations in the blade volume. In the case of carbon, we remark an opposite segregation compared to chromium in the analysed area.

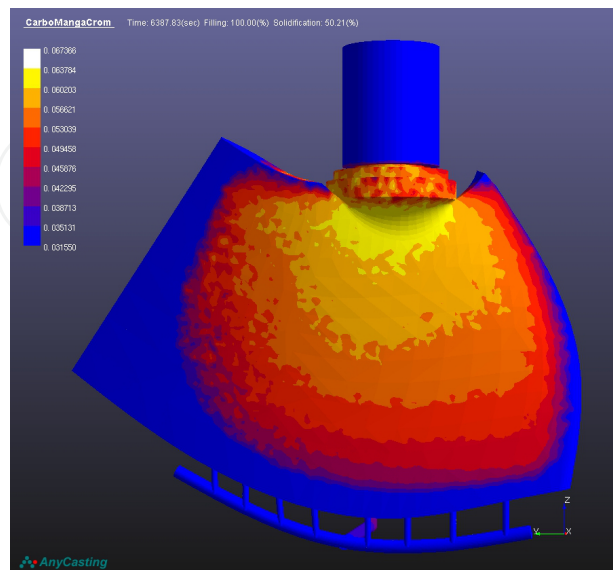


**Figure 47.** Carbon segregation at 50% solidification.

The increase of the carbon percentage and the decrease of chromium concentration by segregation in the passage area between blade and blade axis have a negative influence on mechanical properties. A passage takes place from an austenitic-martensitic structure towards a martensitic-ferritic structure, provoking the decrease of elongation, toughness and tensile strength.

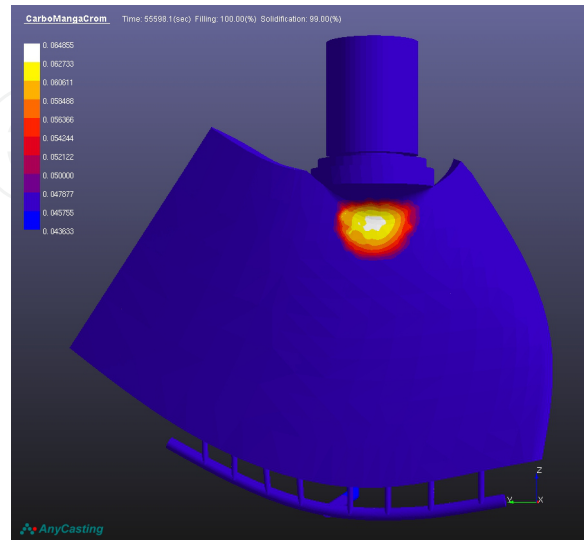


**Figure 48.** Carbon segregation at 100% solidification.

In Figure 48 we remark that the carbon distribution on the blade surface is minimal in the blue zones and maximal in the white zone. The analysis is made by comparing the colours against the colour bar displayed on the left. The inverse carbon segregation also occurs in Figure 49 (carbon segregation at 50% solidification in section) and in Figure 50 (carbon segregation at 100% solidification in section). The increase of the carbon content and the drop of the chromium content by local segregation lead to an accented possibility of manifestation of inter-crystalline corrosion.

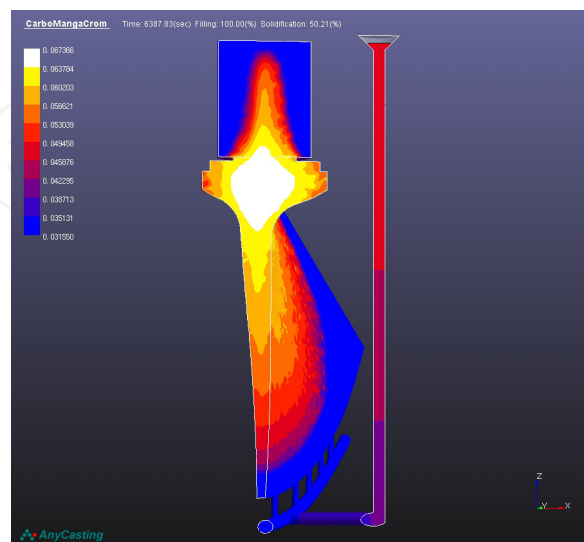


**Figure 49.** Carbon segregation at 50% solidification - vertical section.

Figure 50 shows the carbon distribution in the part volume as being maximum in the white area, at a value of 0.0645, and minimum in the blue zone, at a value of 0.043.

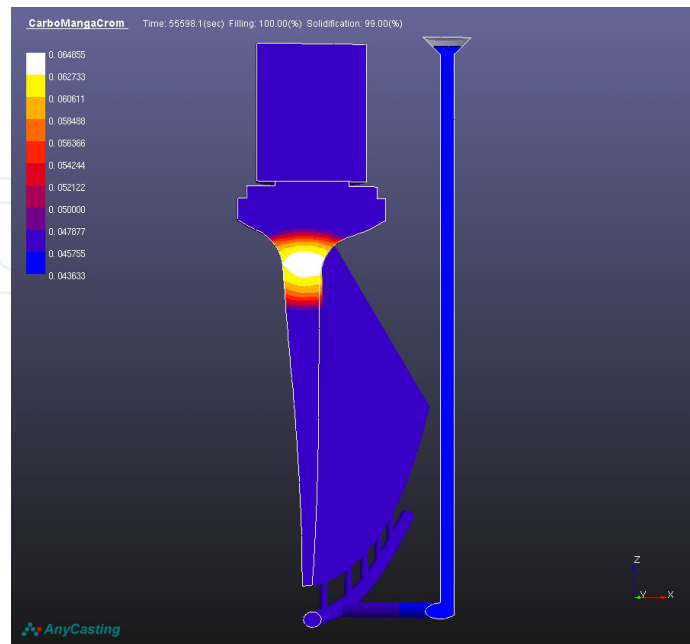


**Figure 50.** Carbon segregation at 100% solidification - vertical section.

#### 4.1. Practical results of the casting of the Kaplan blade part set

We continue by performing analyses with penetrating liquids on the rotor blade in view of identifying casting defects. After the mechanical processing we proceeded to the application of the penetrating substance and of the revelatory. In Figure 51 we can see the effect of penetrating substances on the blade surface.



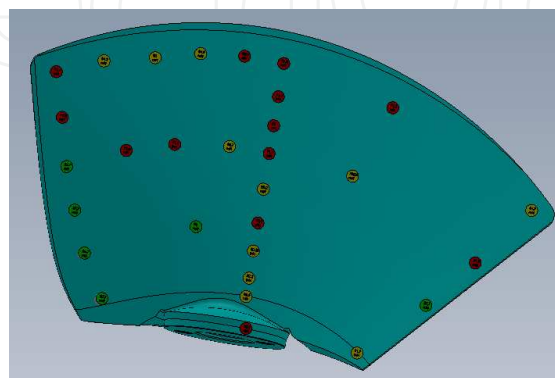
**Figure 51.** Detail in the analysis of the effect of penetrating substances on the blade surface.

Figure 52 exhibits the position of the open air-bubble casting defect in the active exterior side, located near the attack board at around 250 mm under the blade's upper side. The air bubble has smooth walls, does not present dendrite growths, being provoked by the gases from the liquid metal jet, which were not purged during the mould filling and solidification. Around the main bubble and to the lower left side of Figure 52 the reddish coloured zones are in fact several defects such as pores, oxides and rugosities.



**Figure 52.** Position of the bubble open defect and of pores and oxides.

The verification of the conclusions drawn from the blade simulation was done by measurements of inductance, using adequate sensors. The distribution resulted for the of inductance values on the blade surface can be studied in Figure 53, which shows precisely the distribution of inductance values on the blade surface [7].



**Figure 53.** Distribution of inductance values on the blade surface.

The inductance values may be grouped according to colour:

- red – values between 90.05 mH and 93.9 mH; green – values ranging between 86.7 mH and 88.0 mH; yellow – values in the range 80.26 mH and 85.5 mH. In Figure 54 we can see in detail the values of inductance measured in the passage area between the blade flange and the blade block.

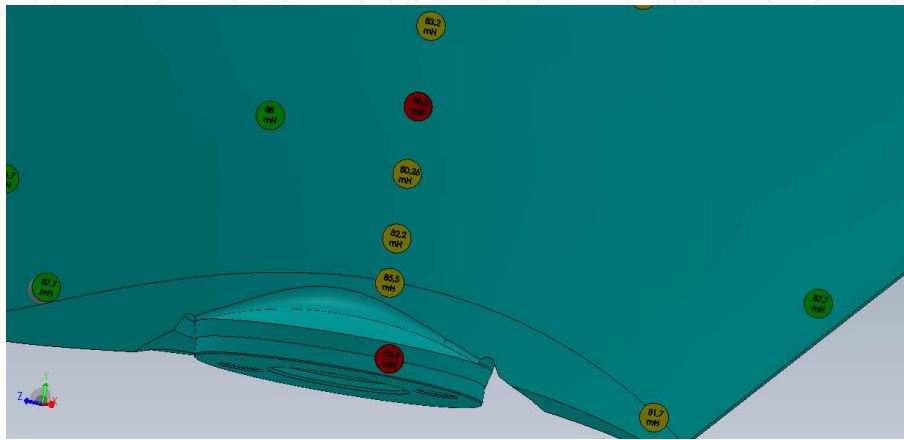


**Figure 54.** Values of inductance measured in the passage area between the blade flange and the blade block.

The inductance values measured in the passage area indicate modifications in the chemical composition and structure of the part volume, which confirms by the results obtained by simulation (see Figures 42-50).

In the figure 55 we can see the martensitic structure with delta ferrite transformations ( $\delta$ ), according to the Scheffler graphic for the chemical composition realized, with the remark that this structure was removed from under the area of the spindle flange at approximately 500 mm. The presence of  $\delta$  ferrite was influenced by a slower cooling speed in that area.

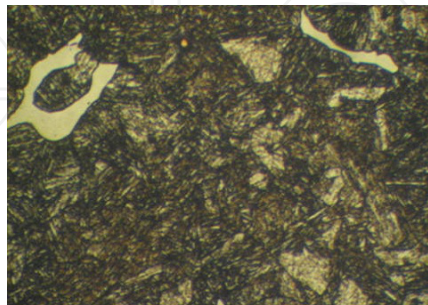


**Figure 55.** Needle martensitic structure with  $\delta$  ferrite -100X.

In figure 56 we can observe a needle martensitic structure, with separations of carbides, typical for the area from the run board, with a smaller thickness of the blade and a greater cooling speed. This area presents enhanced chromium separations.

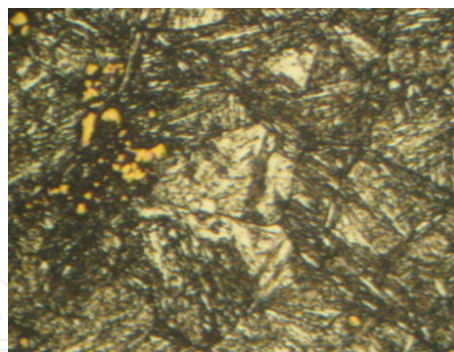


**Figure 56.** Needle martensitic structure with complex carbides -200X.

## 5. Conclusions

Beside the defect presented in Figure 52, other defects are located on the active surface of the blade towards its extremities in the lower left and right sides, middle section and upper side, represented by pores with sizes ranging between 2-3 mm. Other types of defects are oxides, rugositites, fissures on the blade, cracks of the joining between the blade flange and block, preferential segregation of the accompanying and alloying chemical elements (Cr and C). The analysis of the simulation results may lead to the obtaining of solutions meant to enhance the quality of the cast product. Some refer to the technology of steel elaboration and others refer to the improvement of the blade casting process. A measure already presented was feeding the mould by a single feeding network using the system of multi-ingate indirect casting and providing additional feeders in the upper part. The role of these feeders is to retain the driven inclusions and the oxides resulted from the process of steel elaboration and those resulted from the casting process following the secondary oxidation of the liquid metal jet. The module of these feeders can be increased if the elaboration and casting technology are not sufficiently mastered. The conclusions drawn from the research on the improvement of the casting technology for the above parts lead to the manufacture of higher-performance Kaplan turbines from the viewpoint of mechanical properties, with higher resistance to inter-crystalline corrosion and with favourable consequences on life duration. The future researches will be focused on the extension of simulation for a detailed observation of the filling processes, the liquid flow and the solidification of the alloy based on all the criteria specific to this software.

## Author details

Ioan Ruja, Constantin Marta, Doina Frunzăverde and Monica Roșu\*

\*Address all correspondence to: [m.rosu@uem.ro](mailto:m.rosu@uem.ro)

University "Eftimie Murgu" of Reșița, Romania

## References

- [1] Standard: EN 10088 - 2/2005.
- [2] Standard: EN 10088 - 3/2005.
- [3] AnyCasting (2009). Advanced Casting Simulation Software, version 3.10.
- [4] Marta, C. (2011). Aplicatii in AnyCasting / Applications in AnyCasting, Timisoara; Stampa.
- [5] AnyCasting (2009). DataBase, Advanced Casting Simulation Software, version 3.10.
- [6] Marta, C., Suciu, L., & Nedelcu, D. (2009). Simulation of the kaplan rotor hub casting and comparison with the experimental results. *Metalurgia International*, 14(10), 33-38.
- [7] Ignea, A. (1996). Masurarea electrica a marimilor neelectrice /Electrical measurement of non-electrical dimensions. Timisoara: Editura de Vest.

IntechOpen